The Astrophysical Journal, 810:8 (12pp), 2015 September 1 doi:10.1088/0004-637X/810/1/8

NEW INSIGHTS ON THE GALACTIC BULGE INITIAL MASS FUNCTION*

A. Calamida[1], K. C. Sahu[1], S. Casertano[1], J. Anderson[1], S. Cassisi[2], M. Gennaro[1], M. Cignoni[1], T. M. Brown[1], N. Kains[1], H. Ferguson[1], M. Livio[1], H. E. Bond[1,3], R. Buonanno[2,4], W. Clarkson[5], I. Ferraro[6], A. Pietrinferni[2], M. Salaris[7], and J. Valenti[1]

[1] Space Telescope Science Institute, 3700 San Martin Dr., Baltimore, MD 21218, USA; calamida@stsci.edu
[2] INAF—Osservatorio Astronomico di Teramo—Via M. Maggini, sn. I-64100 Teramo, Italy
[3] Department of Astronomy & Astrophysics, Pennsylvania State University, University Park, PA 16802, USA
[4] Dipartimento di Fisica, Universitá di Roma Tor Vergata, Roma, Italy
[5] University of Michigan-Dearborn, USA
[6] INAF—Osservatorio Astronomico di Roma—Via Frascati 33, I-00040 Monteporzio Catone, RM, Italy
[7] Astrophysics Research Institute, Liverpool John Moores University, UK

Received 2015 May 26; accepted 2015 July 22; published 2015 August 24

ABSTRACT

We have derived the Galactic bulge initial mass function (IMF) of the Sagittarius Window Eclipsing Extrasolar Planet Search field in the mass range $0.15 < M/M_{\odot}$ 1.0, using deep photometry collected with the Advanced Camera for Surveys on the *Hubble Space Telescope*. Observations at several epochs, spread over 9 years, allowed us to separate the disk and bulge stars down to very faint magnitudes, $F814W \approx 26$ mag, with a proper-motion accuracy better than 0.5 mas yr^{-1} (20 km s^{-1}). This allowed us to determine the IMF of the pure bulge component uncontaminated by disk stars for this low-reddening field in the Sagittarius window. In deriving the mass function, we took into account the presence of unresolved binaries, errors in photometry, distance modulus and reddening, as well as the metallicity dispersion and the uncertainties caused by adopting different theoretical color–temperature relations. We found that the Galactic bulge IMF can be fitted with two power laws with a break at $M \sim 0.56\ M_{\odot}$, the slope being steeper ($\alpha = -2.41 \pm 0.50$) for the higher masses, and shallower ($\alpha = -1.25 \pm 0.20$) for the lower masses. In the high-mass range, our derived mass function agrees well with the mass function derived for other regions of the bulge. In the low-mass range however, our mass function is slightly shallower, which suggests that separating the disk and bulge components is particularly important in the low-mass range. The slope of the bulge mass function is also similar to the slope of the mass function derived for the disk in the high-mass regime, but the bulge mass function is slightly steeper in the low-mass regime. We used our new mass function to derive stellar mass-to-light values for the Galactic bulge and we obtained $2.1 < M/L_{F814W} < 2.4$ and $3.1 < M/L_{F606W} < 3.6$ according to different assumptions on the slope of the IMF for masses larger than $1M_{\odot}$.

Key words: Galaxy: bulge – stars: evolution

1. INTRODUCTION

The knowledge of the stellar initial mass function (IMF) is a fundamental piece of information in many research areas of astrophysics. From a theoretical point of view, providing tight constraints on the IMF properties in different stellar environments—both in the field and in star clusters—is mandatory to develop a complete and reliable theory of star formation (McKee & Ostriker 2007 and references therein). At the same time, from a phenomenological point of view, the IMF is a fundamental property of stellar populations, and hence a crucial input in any study of galaxy formation and evolution. For instance, it represents an important ingredient in the computations of Population Synthesis models (see Vazdekis et al. 2015 and references therein), and hence it affects our capability to extract the properties of stellar populations such as their luminosity evolution over time, the mass-to-light ratio (*M/L*), the total star formation rate at low and high redshifts, and so on. Therefore, it appears evident that to improve our knowledge of the IMF, or at least to have stronger observational constraints on this crucial ingredient, is of pivotal importance in many astrophysics research fields.

It is particularly important to analyze the properties of the IMF in various stellar environments such as the disk and the bulge of spiral galaxies in order to verify whether the well-known differences (in age and chemical composition) in the stellar populations hosted by the distinct galactic components have an impact on the IMF (Zoccali et al. 2003). An additional reason that makes the study of the IMF in the bulge of spiral galaxies and elliptical galaxies important is due to the possibility that these spheroids could potentially contain the majority of the stellar mass of the universe (see, for instance Fukugita et al. 1998).

As we discuss, the IMF for the Galactic bulge is unlikely to be very different from the present-day mass function (PDMF) below the main-sequence turn-off (MSTO), since most of the star formation in the Galactic bulge happened within about 2 Gyr (Clarkson et al. 2008), with no evidence of star formation after that. So we will refer to the observed PDMF of the Galactic bulge as the IMF in the mass range below the MSTO, which occurs at $\approx 1.0\ M_{\odot}$ for a stellar population with solar metallicity and an age of $t = 11$ Gyr (Calamida et al. 2014, hereafter Paper I).

In spite of the huge improvements achieved in the observational facilities, there is not yet any chance to directly measure the IMF of spheroids outside of our Galaxy. As a consequence, the measurement of the IMF in the Galactic bulge is a fundamental benchmark (or reference point) for any

* Based on observations made with the NASA/ESA *Hubble Space Telescope*, obtained by the Space Telescope Science Institute. STScI is operated by the Association of Universities for Research in Astronomy, Inc., under NASA contract NAS 5-26555.

analysis devoted to investigate this property in extra-galactic spheroids (Calchi Novati et al. 2008).

Concerning the Galactic bulge, the two most recent determinations of the IMF in our spheroid have been performed by Holtzman et al. (1998, hereinafter HO98) and by Zoccali et al. (2000, hereafter ZO00) by taking advantage of the exquisite observational capabilities of the *Hubble Space Telescope* (*HST*). In particular, the analysis performed by ZO00 pushed a step forward the knowledge of the bulge IMF thanks to the use of the Near-infrared camera and Multi-object Spectrometer (NICMOS) available at that time: the derived mass function still represents the deepest measured to date and extends to $\sim$0.15 $M_{\odot}$. They found a power-law slope for the IMF equal to $\alpha = -1.33$ (when a Salpeter IMF would have $\alpha = -2.35$, where $dN/dM = C \times M^{\alpha}$.), with some hint for a possible change of the power slope, $\alpha \approx -2$ at $\sim$0.5 $M_{\odot}$. ZO00 also found that the derived bulge IMF is steeper than that measured for the Galactic disk (Reid & Gizis 1997; Gould et al. 1997). In this context, it is also worth noting that Dutton et al. (2013) have recently used strong lensing and gas kinematics to investigate the existence of possible differences in the properties of the IMF between the disk and the bulge in a sample of spiral galaxies within the Sloan WFC Edge-on Late-type Lens Survey (Treu et al. 2011, SWELLS). As a result they found a significant difference between the bulge IMF and that of the disk, the former being more consistent with a Salpeter IMF, and the latter being more consistent with a Chabrier-like IMF.

On the basis of this evidence, it appears quite appropriate to analyze the properties of the Galactic bulge IMF in different fields of view and using more updated observational data sets. In a previous paper (Calamida et al. 2014, hereinafter Paper I) we have taken advantage of the availability of a huge photometric data set for the low-reddening Sagittarius window in the Galactic bulge collected with the Advanced Camera for Survey (ACS) on board *HST*, to obtain the first unambiguous detection of the white dwarf cooling sequence of the Galactic bulge. In this manuscript, we use the same data to perform a thorough analysis of the IMF in this field of the bulge in order to provide additional, independent insights on the bulge IMF, thus supplementing the results of previous analyses. In this investigation we explore a larger and denser field compared to what was previously observed by HO98 in the Baade's Window and by ZO00 in a field at ($l = 0\overset{\circ}{.}277$, $b = -6\overset{\circ}{.}167$). Most importantly, for the first time we estimate the Galactic bulge IMF based on a clean sample of bulge stars thanks to the very accurate proper motions (PMs) (down to $F814W \approx$ 26 mag) that we were able to measure. Furthermore, we use a statistical approach to apply a correction for the presence of unresolved binaries. We note that the slope of the very low-mass (VLM) range of the IMF is fundamental to estimate the mass budget of a stellar population, since a major fraction of the stellar mass is included in this range and low-mass stars have been hypothesized to contain a significant fraction of the total mass in the universe (Fukugita et al. 1998). It is even more important in the case of the Galactic bulge since this component might include $\approx$20% ($1.8 \times 10^{10} M_{\odot}$) of the mass of the Galaxy (Sofue et al. 2009; Portail et al. 2015).

The structure of the paper is as follows. In Section 2 we discuss the observations and data reduction in detail, while in Section 3 we describe how we selected a clean sample of bulge stars. In Section 4 we present the theoretical mass–luminosity relations we adopted to convert the luminosity functions in mass functions, while Section 5 deals with the different systematics that affect the estimate of the IMF. In Section 6 we compare the derived IMF for the bulge with the disk mass function, and in Section 7 we derive a minimum value for the stellar *M/L* of the Galactic bulge. Section 8 deals with the gravitation microlensing events predicted by the bulge IMF derived in this work, and the conclusions are presented in Section 9.

2. OBSERVATIONS AND DATA REDUCTION

We observed the Sagittarius Window Eclipsing Extrasolar Planet Search (SWEEPS) field ($l = 1\overset{\circ}{.}25$, $b = -2\overset{\circ}{.}65$) in the Galactic bulge in 2004 and again in 2011, 2012 and 2013 with *HST*, using the Wide-Field Channel of ACS (proposals GO-9750, GO-12586, GO-13057, PI: Sahu). The SWEEPS field covers $\approx 3\overset{'}{.}3 \times 3\overset{'}{.}3$ in a region of relatively low extinction in the bulge ($E(B-V) \lesssim 0.6$ mag; Oosterhoff & Ponsen 1968). The 2004 observations were taken in the $F606W$ (wide V) and $F814W$ (wide I) filters over the course of one week (for more details see Sahu et al. 2006). The new data were collected between 2011 and 2013 October, with a $\sim$2-week cadence, for a total of 60 $F606W$- and 61 $F814W$-band images. The two data sets, the 2004 and the 2011–2012–2013 (hereafter 2011–13), were reduced separately by using a software that performs simultaneous point-spread function photometry on all the images. The choice to reduce the two data sets separately is due to the high relative PMs of the disk and bulge stars in this field, caused by the Galactic rotation: the disk star relative PMs peak at $\mu_l \approx 4$ mas yr^{-1}, with a dispersion of $\approx$3 mas yr^{-1}, whereas the bulge motions are centered at $\mu_l \approx 0$ mas yr^{-1}, with a dispersion of $\approx$3 mas yr^{-1} (see Paper I). This means that a substantial fraction ($\sim$30%) of stars would move by more than half a pixel (25 mas) in 9 years.

We calibrated the instrumental photometry to the Vegamag system by adopting the 2004 photometric zero-points, and we obtained a catalog of $\approx$340,000 stars for the 2004 and for the 2011–2013 data sets. The left panel of Figure 1 shows the $F814W$, ($F606W - F814W$) Color–Magnitude Diagrams (CMD) for all the observed main-sequence (MS) stars in the 2011–2013 data set.

The right panel shows the sample completeness as a function of the $F814W$ magnitude. Details on how the completeness was derived are given in Section 2.1. This figure shows that the completeness is $\sim$50% at $F814W \sim 25.5$ mag. The completeness of the $F606W$ magnitude is $\sim$50% at $F606W \sim 28$ mag. The 2004 data set has a very similar completeness, reaching $\sim$50% at $F814W \sim 25.3$ mag and $F606W \sim 28$ mag, respectively.

In order to obtain a clean bulge MS sample to derive the IMF, we estimated the PMs of the stars in this field by combining the astrometry and the photometry of the 2004 and the 2011–2013 data sets. By comparing the positions of stars in the two epochs we estimated PMs for $\approx$200,000 stars down to $F814W \approx 25.5$ mag.

2.1. Artificial Star Tests

To properly characterize the completeness of the measured PMs, the photometric errors and the errors due to the reduction and selection techniques adopted, we performed several artificial star (AS) tests. We created a catalog of $\approx$200,000

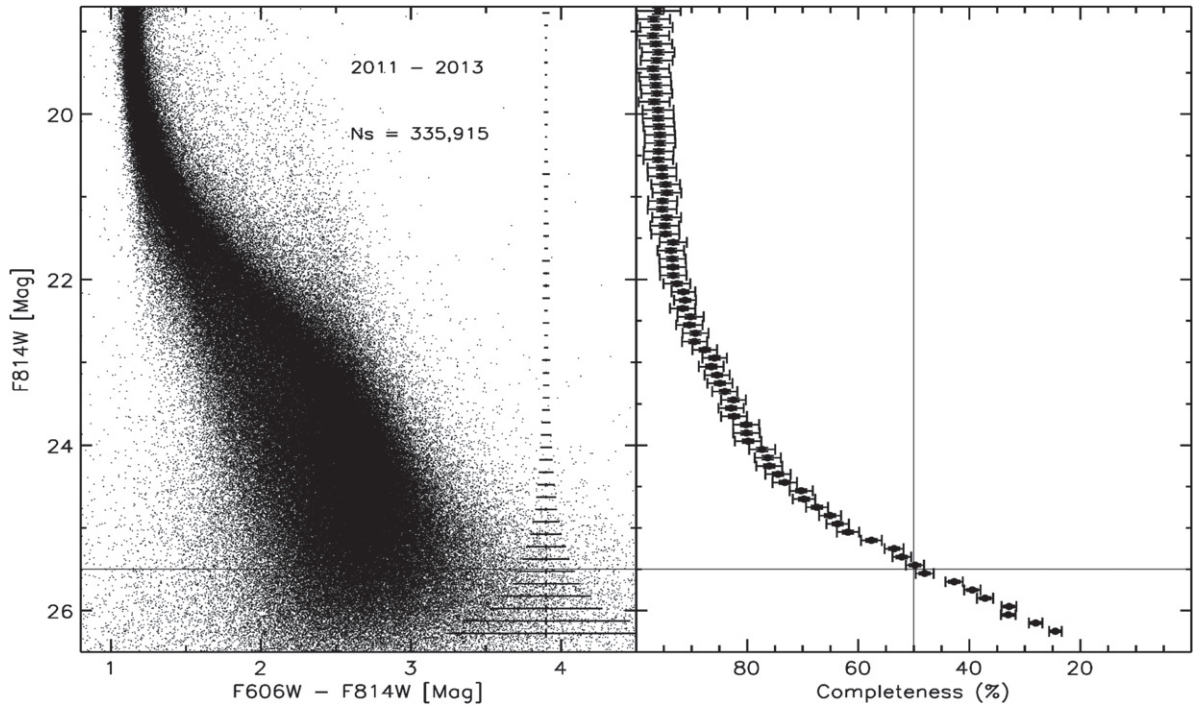

Figure 1. Left: $F814W$, $(F606W - F814W)$ CMD of MS stars in the SWEEPS field based on the 2011–2013 data set. Error bars are also labelled. Right: completeness of MS stars as a function of the $F814W$ magnitude. The horizontal lines in both panels represent the $F814W$ magnitude at which the completeness is 50% and the vertical line in the right panel represents the 50% completeness level.

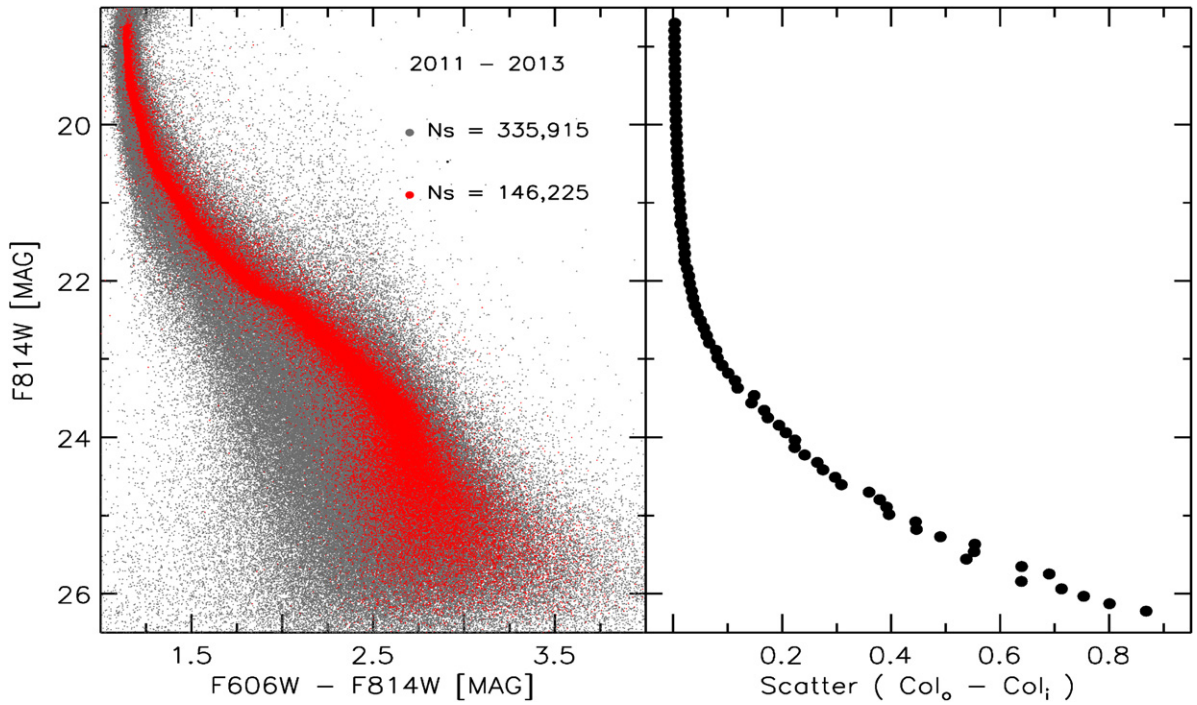

Figure 2. Left: $F814W$, $(F606W - F814W)$ CMD of recovered artificial stars for the 2011–2013 data set (red points). Observed stars are marked with gray points. Stars are selected in magnitude, Δ Mag $\leqslant 0.5$ mag, and in position, $\Delta\, d \leqslant 0.75$ pixel. Right: $(F606W - F814W)$ photometric scatter as a function of the $F814W$ -band magnitude as estimated from the artificial star test.

artificial MS stars, with magnitudes and colors estimated by adopting a ridge line following the MS. We then produced a second AS catalog, by using the same input magnitudes and colors, but applying a PM to each star. We assumed the bulge PM distribution as measured in Paper I, with the distribution centered at $\mu_l \approx 0\,\mathrm{mas\,yr^{-1}}$, and a dispersion of $\approx 3\,\mathrm{mas\,yr^{-1}}$. ASs were added and recovered one by one on every image of the two data sets by using the same reduction procedures adopted earlier. In this way the level of crowding is not affected. In order to estimate the magnitude and color dispersion of the MS due to photometric errors and data reduction systematics, we selected

recovered ASs with $\Delta\mathrm{Mag} = (\mathrm{Mag}_i - \mathrm{Mag}_o) \leqslant 0.5$ mag, and $d = \sqrt{(X_o - X_i)^2 + (Y_o - Y_i)^2} \leqslant 0.75$ pixel, where the quantities with subscript i represent the input, and o represent the output, in both data sets, ending up with a sample of 146,225 stars. We applied this selection because stars which were not recovered in a circle of radius 0.75 pixel can be safely considered not found. The left panel of Figure 2 shows the selected recovered ASs for the 2011–2013 data set (red dots) plotted in the $F814W$, $(F606W - F814W)$ CMD; the observed stars are plotted as well as gray dots. The right panel shows the recovered color spread of the MS as a function of the $F814W$ magnitude. The comparison of the artificial (red dots) and observed (gray dots) CMDs indicates that we are not able to reproduce the entire color spread of the MS by assuming the presence of a single stellar population of solar metallicity and age $t = 11$ Gyr. A metallicity spread of more than 1 dex is present in the SWEEPS bulge field based on medium-resolution spectra of MS turn-off, sub-giant, and red-giant branch stars collected with FLAMES at the Very Large Telescope (see Paper I for more details). The metallicity spread can further broaden the MS, and differential reddening, depth effects as well as binaries might also play a role. It is worth mentioning that most stars in the color and magnitude ranges $2.0 < F606W - F814W < 2.5$ and $18.5 < F814W < 21.5$ mag belong to the (closer) disk population.

In order to estimate the completeness of the measured PMs, we matched the two recovered sets of ASs and compared the output with the input PMs in the direction of both X and Y axes as a function of the two magnitudes. Figure 3 shows this comparison for the X (top panel) and the Y (bottom) axes versus the $F814W$ magnitude. Only stars with $\Delta\mathrm{Mag} \leqslant 0.5$ mag and $d \leqslant 0.75$ pixel are shown. This plot shows that the dispersion of the recovered PMs increases at fainter magnitudes as expected and the accuracy of the measured PMs is better than 0.1 mas yr^{-1} ($\approx$4 km s^{-1} at the distance of the Galactic bulge) at magnitudes brighter than $F814W \leqslant 23$. At $F814W \sim 25$ mag where the completeness is $\gtrsim$50% for both data sets, the recovered PM scatter is $\approx$0.25 mas yr^{-1} ($\approx$10 km s^{-1}) within 3σ uncertainties. This precision will allow us to separate bulge from disk stars down to very faint magnitudes and to characterize the Galactic bulge mass function down to the VLM range, $M < 0.5\ M_{\odot}$.

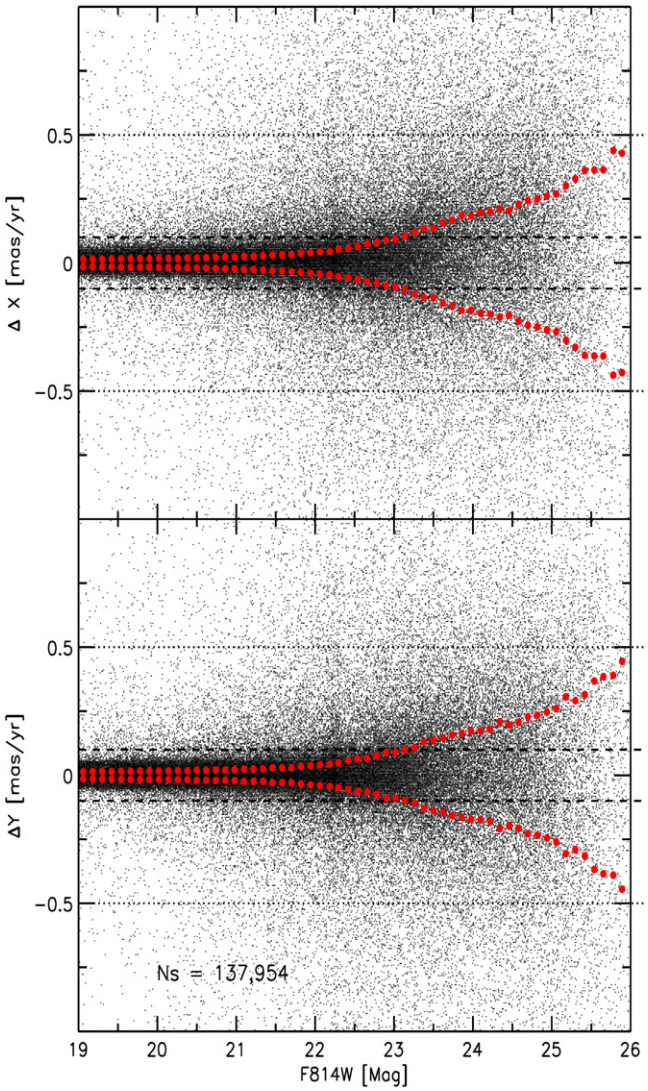

Figure 3. Comparison of Input and Output proper motions in the X (top panel) and Y (bottom) axes of stars recovered in the AS test as a function of the $F814W$ magnitude. The 3σ limit is indicated by the overplotted red dots. Dashed and black dotted lines mark a dispersion of 0.1 and 0.5 mas yr^{-1}, respectively.

3. A CLEAN BULGE MS SAMPLE

We adopted the measured PMs to select a sample of MS stars devoid of disk-star contamination from the 2011–2013 data set. PMs are projected along the Galactic coordinates and we considered stars with $\mu_l \leqslant -2$ mas yr^{-1} to belong to the bulge, following the criteria adopted in Paper I. This selection allowed us to keep $\approx$30% of bulge members while the residual contamination of the sample by disk stars is $\lesssim$1%. We ended up with a sample of 67,765 bulge MS stars.Note that the total contamination by disk stars in the SWEEPS field is $\approx$10%, as shown in the previous work of Clarkson et al. (2008). Figure 4 shows the $F606W$ (left panel) and the $F814W$ (right) versus $(F814W - F606W)$ CMDs of the selected bulge MS stars. The magnitude range covered by MS stars is different when observing with the $F606W$ or the $F814W$ filter, decreasing from $\sim$8.5 to 7 mag. This happens because VLM MS stars are cooler and thus more luminous at longer wavelengths.

The CMDs of Figure 4 show that the color spread of the MS did not substantially decrease compared to the CMD of Figure 1, confirming that most of the color dispersion is due to the spread in metallicity, the presence of some amount of differential reddening, depth effects and binaries.

Figure 5 shows the observed PM-cleaned bulge MS luminosity function (dashed line) based on the $F814W$ magnitude for the stars plotted in the CMDs of Figure 4. The completeness measured from the AS test is used to correct the number of observed stars per magnitude bin and the corrected luminosity function is over-plotted in the same figure with a solid line. We applied the completeness correction by binning on the observed magnitudes; in this way we take into account the uncertainties due to the photometric errors moving the stars among the magnitude bins. The $F814W$-band corrected luminosity function of Figure 5 extends from just below the bulge MSTO at $F814W \sim 19$ mag down to $F814W \sim 26$ mag, where the completeness level is $\sim$30%. A similar luminosity function is obtained by adopting the $F606W$ magnitude.

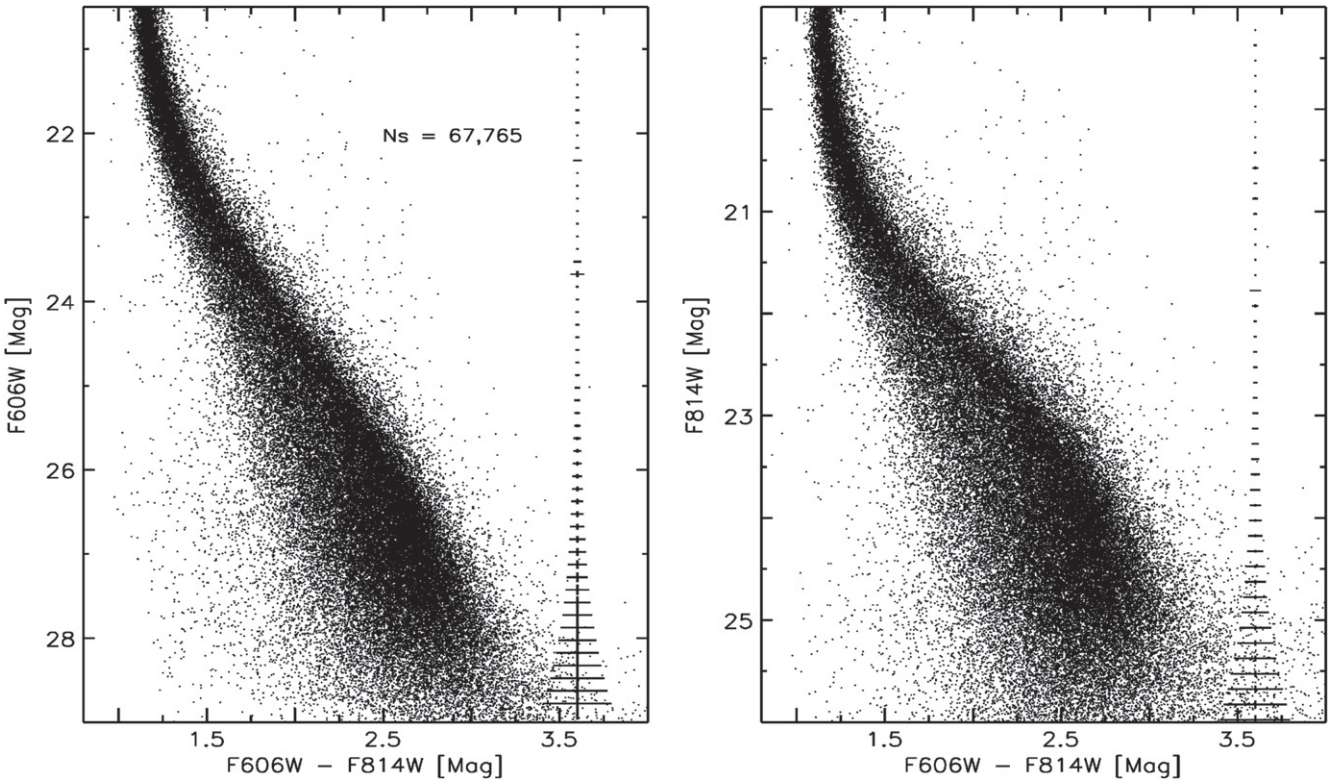

Figure 4. Left: PM-cleaned bulge MS $F606W$, $F606W - F814W$ CMD; note that 70% of the bulge stars were rejected because of the PM selection. Error bars are also labelled. Right: same stars plotted on the $F814W$, $F606W - F814W$ CMD.

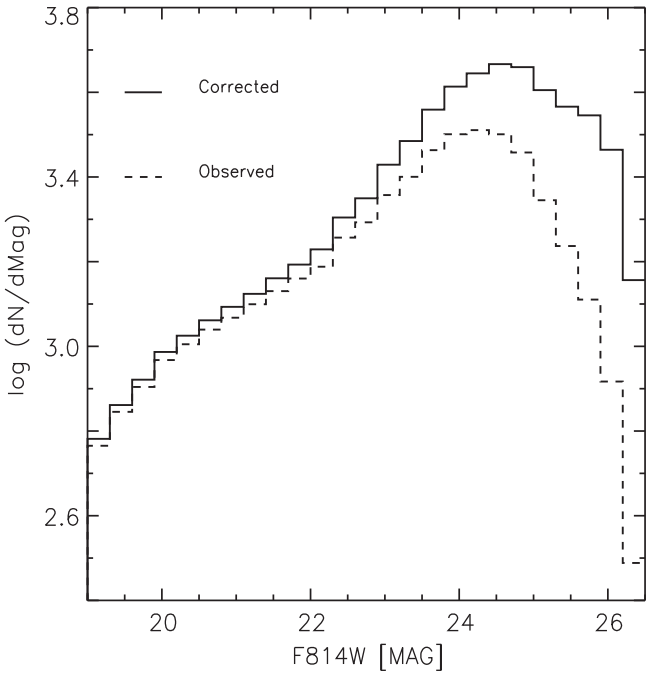

Figure 5. $F814W$-band observed luminosity function for the Galactic PM-cleaned bulge MS stars (dashed line) and the luminosity function corrected for completeness (solid line).

4. THE MASS–LUMINOSITY RELATION

In Paper I we used the BaSTI[8] (Pietrinferni et al. 2004, 2006) stellar-evolution database to fit isochrones to the bulge CMD. In order to extend the BaSTI isochrones[9] to the range of very-low-mass stars ($M < 0.5M_{\odot}$) we computed VLM stellar models for exactly the same chemical composition of the BaSTI ones, by adopting the same physical inputs used in (Cassisi et al. 2000, hereafter CA00). We note that, the accuracy and reliability of the BaSTI models and their extension to the VLM stellar regime have been extensively tested by comparing them with observed CMDs and mass–luminosity (M–L) data sets for both field and cluster stars. As a result, a very good level of agreement has been obtained with the various observational constraints (Cassisi et al. 2000, 2009, 2014; Bedin et al. 2009; Cassisi & Salaris 2011). Since the VLM stellar models have been computed by using a different physical framework compared to the models of more massive stars in the BaSTI library (see Pietrinferni et al. 2004 and CA00 for more details on this issue) one can expect that, in the stellar mass regime corresponding to the transition between the BaSTI and the VLM stellar models occurring at about $\sim 0.6M_{\odot}$, some small mismatch in surface luminosity and effective temperature at a given mass is possible. Since in retrieving the IMF one has to rely on the first derivative of the theoretical M–L relation, it is important to eliminate any such discontinuity in the M–L relation (Kroupa & Tout 1997). To this aim, we devoted a huge effort—which included computing additional stellar models using both the physical inputs adopted for the BaSTI library and that used by CA00—in order to match the two model data sets at the stellar mass with (almost) the same luminosity and effective temperature.

[8] http://albione.oa-teramo.inaf.it/

[9] In their standard format the minimum initial mass in the BaSTI isochrones is equal to 0.5 $M_{\odot}$. The BaSTI isochrones extended in the VLM star regime are available at the BaSTI URL repository.

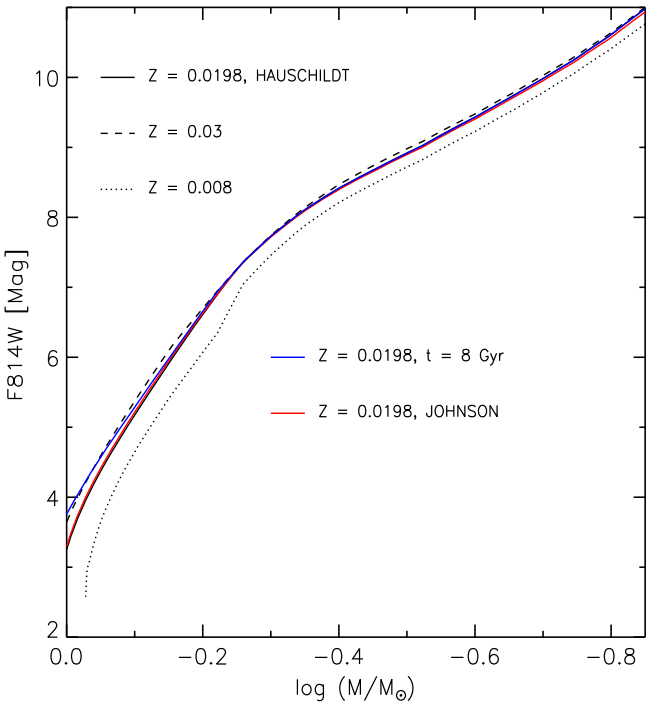

Figure 6. Theoretical mass–luminosity relations for different metallicities, ages, and color–temperature relations.

The evolutionary predictions were transformed from the theoretical to the observational plane by adopting the color–$T_{\rm eff}$ relations and bolometric correction scale for the ACS filters provided by Hauschildt et al. (1999) for $T_{\rm eff} \leqslant 10{,}000$ K, while at larger $T_{\rm eff}$ we adopted the relations published by Bedin et al. (2005).

Figure 6 shows selected scaled-solar isochrones[10] for the same age, $t = 11$ Gyr, and different metallicities, $Z = 0.008$, 0.0198, 0.03, plotted in the $F814W$ versus $\log(M/M_{\odot})$ plane. We selected models with this age and abundances based on the fit of the bulge CMD performed in Paper I (see Figure 2) and on the spectroscopic metallicity distribution for this field. In the same plot a solar metallicity isochrone but for an age of 8 Gyr is also shown (blue solid line). As expected, in the explored age and stellar mass range, the *M–L* is completely unaffected by an age change. In order to check the impact on the adopted *M–L* relation related to the use of a different bolometric correction scale, we also plotted the 11 Gyr, solar metallicity isochrone transferred in the observational plane by using the standard Johnson bolometric corrections provided by Pietrinferni et al. (2004) and the transformations from the Johnson to the *HST* photometric system by Sirianni et al. (2005, red solid).

The five mass–luminosity relations all show a slight change of the slope around $\log(M/M_{\odot}) \approx -0.3$ ($M \approx 0.5\,M_{\odot}$). This inflection point is due to the molecular Hydrogen recombination occurring at a mass equal to $\approx 0.5 M_{\odot}$; the formation of the H_2 molecule changes the value of the adiabatic gradient and, hence, the stellar structure thermal stratification (see Cassisi et al. 2000 and references therein).

Figure 6 also shows the impact of using various metallicities or ages for the selected *M–L* relation. As discussed, for old ages, $t \geqslant 8$ Gyr, suitable for the Galactic bulge population under scrutiny, the exact value of the selected age is quite irrelevant. On the other hand, the change in the mass derived (at a fixed magnitude) using two different mass–luminosity relations corresponding to $Z = 0.008$ (which is the most metal-poor chemical composition we selected) and $Z = 0.03$ (which is our most metal-rich composition) is only about $\approx$0.04–0.08 $M_{\odot}$ in the high-mass range ($M > 0.5\,M_{\odot}$), and $\approx$0.02–0.04 $M_{\odot}$ in the lower-mass range. The spectroscopic metallicity distribution we derived for the SWEEPS field, as discussed in Section 3.1 and Paper I, spans a range of metallicity from $[M/H] \sim -0.8$ to $\sim$0.6, i.e., more than 1 dex. However, the distribution shows three peaks at $[M/H] \sim -0.4$, 0.0 and 0.3 and most of the stars, $\sim$85%, are included in the range $-0.5 < [M/H] < 0.5$. We can then safely assume the aforementioned metallicity values, $Z = 0.008$ and $Z = 0.03$, corresponding to the more metal-poor and the more metal-rich peaks of the distribution, to test the effect of metallicity on the mass estimate. However, we also tested the effect of further decreasing the metallicity of the adopted models, by using an isochrone for $Z = 0.002$ and the same age, $t = 11$ Gyr, to convert luminosities into masses. In this case, the mass estimate changes by $\sim$17% in the entire mass range, when going from the more metal-rich model, $Z = 0.03$, to the more metal-poor, $Z = 0.002$. For a small fraction of stars in our field, less than $\sim$10%, the mass estimate will have a $\sim$5% larger uncertainty.

The impact of using a different bolometric correction scale for transferring the models from the theoretical to the observational plane in the derived masses is smaller and of the order of $\approx$0.005 $M_{\odot}$ in the entire mass regime.

5. THE GALACTIC BULGE IMF

The mass–luminosity relation we obtained for MS stars by using BaSTI isochrones is only the first step toward determining the IMF of the Galactic bulge. Uncertainties due to the assumed distance and reddening, presence of differential reddening, metallicity dispersion, depth effects, and the presence of binaries need to be taken into account.

Following Sahu et al. (2006) and Paper I, we fitted the bulge CMD using a distance modulus of $\mu_0 = 14.45$ mag (Sahu et al. 2006) and a mean reddening of $E(B-V) = 0.5$ mag and a standard reddening law Extinction coefficients for the WFC filters are estimated by applying the Cardelli et al. (1989) reddening relations and by adopting a standard reddening law, $R_V = A_V/E(B-V) = 3.1$, finding $A_{F606W} = 0.922 \times A_V$, $A_{F814W} = 0.55 \times A_V$, and $E(F606W - F814W) = 1.14 \times E(B-V)$. It is worth mentioning that if we use the reddening value estimated by Nataf et al. (2013) for the SWEEPS field, $E(V-I) = 0.79$, and their extinction curve, $R_V = A_V/E(B-V) = 2.5$, we obtain $E(B-V) = 0.47$, in good agreement with the value we assumed.

We used the $F814W$-band luminosity function to probe the bulge IMF since MS stars are brighter at redder colors and so the photometry in this filter is more complete and accurate than in the $F606W$ filter for the same mass (see the CMDs in Figure 4). We converted observed magnitudes into masses using the mass–luminosity relation for solar metallicity, $Z = 0.0198$, and for an age of $t = 11$ Gyr, transformed by

[10] Our referee correctly pointed out that bulge stars appear to be α-enhanced up to about solar metallicity (Zoccali et al. 2008; Gonzalez et al. 2011; Johnson et al. 2011, 2013). However, we decided in present work to adopt scaled-solar models due to the lack of suitable alpha-enhanced VLM star sequences in a wide metallicity range. This notwithstanding, we note that all the comparisons performed in present paper are performed at constant global metallicity (and not at constant [Fe/H] and it is well known that α-enhanced stellar models are nicely mimicked by scaled-solar one with the same global metallicity (see, e.g., Pietrinferni et al. 2006 and references therein).

using the color–$T_{\rm eff}$ relations by Hauschildt et al. (1999). As we showed in the previous section, age does not significantly affect the mass–luminosity relation for $t \geqslant 8$ Gyr, and observational evidence shows that most bulge stars in our field are older than 8 Gyr (Clarkson et al. 2008, Paper I).

In order to estimate the effect of dispersion in metallicity, we computed the difference in the masses derived by adopting three different metallicities: solar ($Z = 0.00198$), metal-rich ($Z = 0.03$), and metal-poor ($Z = 0.008$). For magnitudes in the range $18.0 < F814W < 26$, this changes the inferred masses by 0.02–0.08 $M_{\odot}$, resulting in an uncertainty of ≈8% in mass.

We also varied the assumed distance modulus by 0.2 mag, from 14.35 to 14.55 mag, corresponding to a depth of ∼1 Kpc, and the extinction, $E(B - V)$, from 0.45 up to 0.55 mag. Both the distance and reddening uncertainty affects the derived masses by ≈0.01 $M_{\odot}$ over the entire mass range, i.e., 1%–5%. Similarly, adopting different color–$T_{\rm eff}$ relations changes the derived massed by less than 2%.

By summing in quadrature the uncertainties related to the parameters of the bulge CMD as fitted to our data, including metallicity, distance, reddening, and color–$T_{\rm eff}$ relations, we obtain a final systematic uncertainty on the mass estimate for each star. This uncertainty varies depending on the inferred mass and is carried through the remainder of the analysis.

5.1. The Effect of Unresolved Binaries

Unresolved binaries, i.e., the expected presence of equal or lower-mass binary companions for many of the MS stars we observe, are likely to affect the inferred IMF of the bulge especially at lower masses, such as $M < 0.5 M_{\odot}$ (see, e.g., Kroupa et al. 1991 and Kroupa 2001).

The availability of photometry in two different filters for a large fraction of our stars potentially allows us to correct for the effect of unresolved binaries, as binary systems will be somewhat redder than single stars of the same apparent brightness. However, the photometry, in particular at the faint end, is not sufficiently accurate for a direct identification of individual binary systems; our correction must therefore be probabilistic.

Both the fraction of binaries and the distribution of mass ratios for the Galactic bulge are not well constrained. However, in Paper I we showed that there is evidence for a substantial fraction of He-core white dwarfs in the bulge based on the color dispersion of the cooling sequence and the comparison between star counts and predicted evolutionary lifetimes. According to standard stellar evolution models, He-core white dwarfs can only be produced in a Hubble time by stars experiencing extreme mass-loss events, such as in compact binaries. Indeed, in Paper I we reported our finding of two dwarf novae in outburst and five candidate cataclysmic variables in the same field, both of which are characteristic of a population of binaries. Our evidence at the time suggested that the Galactic bulge has a fraction of binaries of larger than 30%.

For the present analysis, we assume that the distribution of mass ratios of binary stars in the bulge follows the distribution derived by (Duquennoy & Mayor 1991, hereafter DM) for a sample of 164 F- and G-dwarf stars in the solar neighborhood. The distribution is a log-normal and it is described by the functional form:

$$\xi(q) = Ce^{\left\{\frac{-(q-\mu)^2}{2\sigma_q^2}\right\}} \quad (1)$$

in the interval [0, 1], where $q = M_2/M_1$, $\mu = 0.23$ and $\sigma_q = 0.42$ and $C = 10{,}900$ for our sample of bulge stars.

We also repeated the experiment by assuming a flat mass-ratio distribution similar to the distribution found by Raghavan et al. (2010) based on data for 454 F- to K-dwarf stars within 25 pc of the Sun.

In a simplified Bayesian approach, we use the fraction of binaries and the distribution of mass ratios from Equation (2) as a prior for the presence and mass of binary companions, and then use the observed photometry to determine the posterior probability distribution of companion mass for each star in our sample.

For simplicity, for each observed bulge star we consider 11 discrete options J, $J = 0, ..., 10$. The option $J = 0$ implies a single star, $J > 0$ implies a binary system with mass ratio $q_J = J/10$. The prior probability Pr_J of each option is consistent with the DM distribution with an overall binary fraction of 50%; thus $Pr_0 = 0.5$, $Pr_{1-10} = 0.07$, 0.072, 0.07, 0.063, 0.06, 0.05, 0.04, 0.035, 0.025, 0.015.

For each value of J, the total system mass $(M_T)_J = (M_1)_J + (M_2)_J$ is chosen so as to match the total flux in the $F814W$ filter, using the appropriate mass–luminosity relation for age, metallicity and distance for both components (or only one component if $J = 0$). We then compute the likelihood $P_{\rm D|M} = P(\text{Data}|\text{Model})$ of the measured total flux in the $F814W$ filter, given the model, using a Gaussian distribution for the flux with the realistic photometric errors derived above. To the photometric errors derived from the AS tests, we added errors due to the presence of a metallicity spread, differential reddening and depth effects. These have been derived by using mass–luminosity relations for different metallicities, and by varying the distance modulus of 0.2 mag, and reddening of 0.1 mag, as described in Section 5. To each observed star we thus assign a probability distribution function of the component masses over the allowed values of the mass ratio between components, according to the classic Bayes formula: $P_J = Pr_J * P_{\rm D|M}/P(\text{Data})$, where $P(\text{Data})$ is a normalization factor chosen to take into account the estimated completeness correction.

Finally, we generate multiple realizations of the full stellar mass function by randomly drawing stellar distributions with the probabilities thus determined. This procedure allows us to better understand and quantify the uncertainties arising from the correlated nature of the probabilities for each object (e.g., only one value of the mass ratio can be selected for each system).

In practice, larger mass ratios q_J generally correspond to redder $F606W - F814W$ colors at given $F814W$-band flux; thus stars that lie red-ward of the MS of Figure 4 will generally favor larger mass ratios, while stars located near the MS will be consistent with a single star or a low-mass binary companion which contributes little to the total flux. However, note that for many stars the photometric error is large enough that photometry (through the term $P_{\rm D|M}$) does not provide a strong discriminant; for such cases, the final probability P_J for each option is the same as the prior probability Pr_J. By not taking into account the photometric color information, for instance,

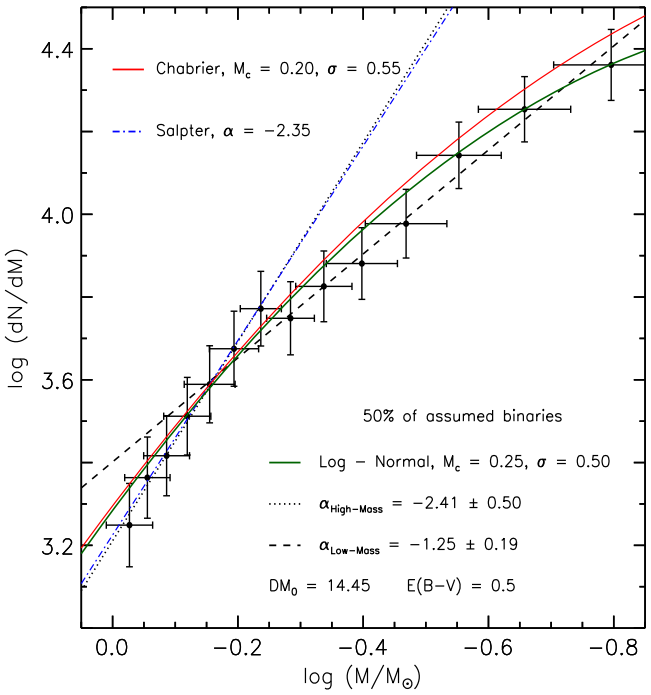

Figure 7. IMF of the Galactic bulge. The two power laws that fit the IMF are over plotted, for a slope $\alpha = -2.41 \pm 0.50$ (dotted line) and $\alpha = 1.25 \pm 0.19$ (dashed), together with a log-normal function with $M_c = 0.25$ and $\sigma = 0.50$ (green solid). The Salpeter mass function (blue dash–dotted line) and the Chabrier log-normal function (red dashed double dotted) are also shown. Error bars are displayed.

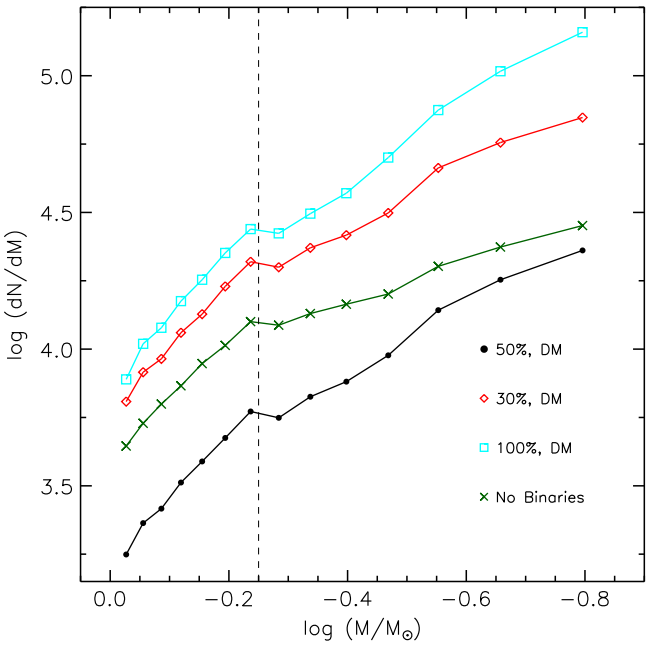

Figure 8. IMFs of the Galactic bulge derived by assuming different fraction of binaries and a DM mass-ratio distribution for the binaries.

the distribution changes by ≈2%–7% in the VLM range, and by less than 1% at higher masses, i.e., $M > 0.5\ M_\odot$.

As discussed in the following subsection, undetected binaries have a substantial impact in the inferred mass function, especially below ≈0.5 $M_\odot$. However, we must remark that the distribution of binary properties is uncertain and poorly constrained by the data at hand; changing the assumed binary fraction and the a priori distribution of mass ratios would also alter the derived mass function, as we show in Section 5.2.

The treatment above is somewhat simplified in comparison with a fully Bayesian approach, in which we would consider fully the uncertainties in in the parameters of the model (metallicity, distance, reddening variation), using for each an appropriate distribution rather than the "best" values. We defer this more complex and computationally expensive approach to the analysis of the full data set, including one more season of photometry and eleven additional fields.

5.2. Discussion

One of the realizations of the Galactic bulge IMF is shown in Figure 7. Error bars also include the uncertainties that come from statistical noise in the star counts. We generated 10,000 realizations of the same mass function and fitted them by adopting two power laws. The fit was performed by varying the mass break-point in the range $-0.2 \leqslant \log(M/M_\odot) \leqslant -0.3$ and the lowest chi-square fit resulted with for a value of $\log(M/M_\odot) = -0.25$ ($M = 0.56\ M_\odot$). The best estimate of the power-law slopes are $\alpha = -2.41 \pm 0.50$ (dotted line) for higher masses, and $\alpha = -1.25 \pm 0.19$ (dashed) for lower masses, where $dN/dM = CM^\alpha$.

We also fitted the Galactic bulge IMF by using a log-normal function described by the functional form:

$$\xi(\log M) = C \exp\left\{-\frac{\left[\log(M) - \log(M_c)\right]^2}{2\sigma^2}\right\} \qquad (2)$$

with $M_c = 0.25 \pm 0.07$ and $\sigma = 0.50 \pm 0.01$ (solid green line in Figure 7).

The power-law slope for the high-mass range ($M > 0.56\ M_\odot$) agrees very well with the Salpeter IMF ($\alpha = -2.35$) derived for solar neighborhood stars in the mass range 0.3–10 $M_\odot$ (blue dash–dotted line in Figure 7). The log-normal mass function derived for disk stars closer than 8 pc in the mass range 0.08–1.0 $M_\odot$ by Chabrier (2003, 2005) has $M_c = 0.20$ and $\sigma = 0.55$ (dash-double dotted red line) and agrees well with our Galactic bulge IMF.

We derived the IMFs using the same method described in the previous section for different values of binary fraction, assuming a flat distribution of mass ratios, and a distribution given by DM. Figure 8 shows one realization for each of the IMFs derived for different binary fractions and the DM mass-ratio distribution. In general, the IMF has two distinct slopes in the low- and high-mass ranges, and the slopes have only a weak dependence on the assumed mass-ratio distribution for the binaries. If we assume the DM mass-ratio distribution for the binary components, the slopes of the IMF at higher masses are −2.25, −2.36, −2.41, and −2.53, for a bulge binary fraction of 0%, 30%, 50%, and 100%, respectively. If we assume a flat mass-ratio distribution, the slopes change only by 1%–4% for binary mass fractions of 0%–100%. The corresponding slopes in the low-mass range are −0.89, −1.12, −1.25, and −1.51 for the DM mass-ratio distribution, and they change by 3%–4% for a flat mass-ratio distribution. Full details including the error bars are given in Table 1. These results indicate that the effect of the presence of unresolved binaries is more pronounced in the low-mass range (∼50%), than in the high-mass range (∼12%). In the rest of the

Table 1
Power-law Slopes of The IMFs Derived By Assuming Different Binary Fractions and Mass-ratio Distributions for the Galactic Bulge

Binary fraction	Mass-ratio	$\alpha_{\rm High}$	$\alpha_{\rm Low}$
0	...	-2.25 ± 0.50	-0.89 ± 0.20
30	DM	-2.36 ± 0.51	-1.12 ± 0.19
50	DM	-2.41 ± 0.50	-1.25 ± 0.19
100	DM	-2.53 ± 0.51	-1.51 ± 0.20
30	Flat	-2.39 ± 0.51	-1.16 ± 0.19
50	Flat	-2.45 ± 0.51	-1.29 ± 0.19
100	Flat	-2.62 ± 0.52	-1.55 ± 0.20

discussion, we use the IMF derived by assuming a binary fraction of 50% and a DM mass-ratio distribution. As discussed in Section 5.1, the presence of a substantial fraction of He-core WDs in the Galactic bulge suggests that the fraction of binaries in the bulge is larger than 30%.

6. COMPARISON WITH OTHER IMFS

6.1. Galactic Bulge

The Galactic bulge mass function was first measured by HO98 based on a set of observations of the Baade's window ($l = 1^\circ$, $b = -4^\circ$) collected with the Wide Field Planetary Camera 2 (WFPC2) on board *HST*. These data allowed them to derive a luminosity function down to $F814W \sim 24.3$, corresponding to $M \sim 0.3\ M_\odot$. No information on PMs was available, so disk stars are included in their study.But they applied a correction for the presence of unresolved binaries and found that the IMF of the bulge has a power-law slope of $\alpha = -2.2$ in the high-mass range. The slope of the IMF flattens at $\sim 0.7 M_\odot$, with $\alpha = -0.9$ for a fraction of binaries of 0% and -1.3 for 50% (see Table 2). HO98 result for an assumed fraction of binaries of 50% agrees quite well, within the uncertainties, with what we obtained in our analysis for the same assumption on binaries, but the changing of power-law slope occurs at lower masses, $\sim 0.56\ M_\odot$, in our bulge IMF.

A second study on the Galactic bulge mass function was published by ZO00, based on a set of observations collected in the $F110W$ and $F160W$ filters with NICMOS on board *HST*, covering a $22\farcs5 \times 22\farcs5$ field of view in a region of the bulge South of the Baade's window ($l = 0\fdg277$, $b = -6\fdg167$). To convert magnitudes to masses they used a mass–luminosity relation based on the same stellar models adopted in this investigation. They also did not have propel-motion information to separate bulge from disk stars, nor did they apply a correction for the presence of unresolved binaries. However, ZO00 applied an overall reduction of the luminosity function by 11% for magnitudes brighter than $J < 17$, to take into account the contamination by disk stars. By fitting the IMF with a single power law they obtained a slope of $\alpha = -1.33 \pm 0.07$, over the mass range $0.15 < M/M_\odot < 1.0$, while by using two different power laws they obtained $\alpha = -2.00 \pm 0.23$ for masses $M > 0.5\ M_\odot$, and $\alpha = -1.43 \pm 0.13$ for lower masses (see Table 2). If we fit our IMF by using a single power law for the entire mass range ($0.15 < M/M_\odot < 1.0$), we obtain a range of slopes from $\alpha = -1.14 \pm 0.10$ for no binaries to $\alpha = -1.56 \pm 0.10$ for 100% of binaries. The slope of the IMF not corrected for the presence of unresolved binaries is then shallower compared to the slope of the IMF obtained by ZO00 (-1.14 versus -1.33). Moreover, the same IMF shows a much shallower slope in the low-mass regime compared to ZO00 mass function (-0.89 versus -1.43). This discrepancy might be due to the residual contamination by disk stars of ZO00 sample. Part of the difference could also be due to an intrinsic difference of stars observed by ZO00 and stars in the SWEEPS field. From spectra collected by our group the stars in this region of the bulge have a similar metallicity distribution as the stars in the Baade's Window, with main peaks at $[M/H] \approx -0.4$, 0, and 0.3 (Hill et al. 2011; Bensby et al. 2013; Ness et al. 2013). The metallicity distribution of the region of the Galactic bulge observed by ZO00 shows a decrease in the fraction of metal-rich stars, with the average metallicity decreasing from [Fe/H] $\sim +0.03$ in the Baade's window down to [Fe/H] ~ -0.12 (Zoccali et al. 2008). However, such a small difference in the metallicity distribution cannot account for a $\sim$20% difference in the IMF slope.

6.2. Galactic Disk

The Galactic disk mass function has been constrained in the low-mass regime down to the hydrogen-burning limit and in the brown dwarf regime by various studies. Salpeter (1955) derived the "original mass function" for solar neighborhood stars in the range $0.3 \lesssim M/M_\odot \lesssim 10$ and fitted it by using a single power-law with a slope of $\alpha = -2.35$. Later studies found that the disk mass function can be reproduced either by a segmented power law or by a log-normal function. Table 2 lists the power law slopes and the characteristic masses and sigmas used by different studies to fit the Galactic disk mass function. Kroupa et al. (1993) and later Kroupa (2001) derived the IMF for disk stars within 5.2 pc of the Sun by taking into account a correction for the presence of unresolved binaries and fitting it with a power law with a slope of $\alpha = -2.2 \pm 0.3$ in the mass range $0.5 < M/M_\odot < 1.0$ and of $\alpha = -1.3 \pm 0.5$ in the range $0.08 < M/M_\odot < 0.5$. Gould et al. (1997) based their study of the Galactic disk mass function on photometry collected with the WFPC2 and WFPC1 on board *HST*. They observed a sample of 337 stars distributed in different regions of the disk and found a mass function with a slope close to Salpeter, $\alpha \sim -2.2$, for masses in the range $0.6 < M/M_\odot < 1.0$, and $\alpha \sim -0.9$ for lower masses. Reid et al. (2002) observed a sample of 558 MS stars in the solar neighborhood in the mass range $0.1 < M/M_\odot < 3.0$ and found that a power law with a slope of $\alpha = -1.3$ fits the mass function in the low-mass range, i.e., for stars with $M < 0.7\ M_\odot$. Chabrier (2005) adopted a log-normal function to fit the Galactic disk IMF for single stars in the mass range $0.08 < M/M_\odot < 1.0$, and found a characteristic mass $M_c = 0.20 \pm 0.02$, and $\sigma = 0.55 \pm 0.05$.

More recent analyses based on the Sloan Digital Sky Survey and the 2MASS data confirmed previous results, showing that the Galactic disk mass function can be reproduced either by assuming a segmented power law with slopes of $\alpha = -2.04/-2.66$ and $\alpha = -0.8/-0.98$, for the high- and low-mass range, respectively, or by a log-normal function with $M_c = 0.20/0.50, \sigma = 0.22/0.37$ (Covey et al. 2008; Bochanski et al. 2010).

The IMF we derived for the Galactic bulge is in very good agreement, within uncertainties, with the mass function obtained by Kroupa (2001) and Chabrier (2005) for the disk. On the other hand, the mass functions derived for the disk by Covey et al. (2008) and Bochanski et al. (2010) have a slightly shallower slope compared to our bulge IMF in the low-mass regime (see Table 2), although the two mass functions would

Table 2
List of The Different Mass Functions Derived for the Galactic Bulge and Disk

Reference	Mass Range	$\alpha_{\rm High}$	$\alpha_{\rm Low}$	$M_{\rm break}$	α	$M_{\rm c}$	σ
			Galactic Bulge				
This work	0.15–1.0	-2.41 ± 0.50	-1.25 ± 0.19	0.56	…	0.25 ± 0.07	0.50 ± 0.01
Holtzman et al. (1998)	0.30–1.0	-2.2	-1.3	0.7	…	…	…
Zoccali et al. (2000)	0.15–1.0	...	…	...	-1.33 ± 0.07	…	…
			Galactic Disk				
Salpeter (1955)	0.30–10	…	…	…	-2.35	…	…
Kroupa et al. (1993), Kroupa (2001)	0.08–1.0	-2.3 ± 0.3	-1.3 ± 0.5	0.5	…	…	…
Gould et al. (1997)	0.08–1.0	-2.2	-0.9	0.6	…	…	…
Reid et al. (2002)	0.10–3.0	…	…	…	-1.3	…	…
Chabrier (2005)	0.10–1.0	…	…	…	…	0.20 ± 0.02	0.55 ± 0.05
Covey et al. (2008)	0.10–0.7	-2.04	-0.8	0.32	-1.1	0.20–0.50	0.22–0.37
Bochanski et al. (2010)	0.10–0.8	-2.66 ± 0.10	-0.98 ± 0.10	0.32	…	0.18 ± 0.02	0.34 ± 0.05

agree at lower masses by assuming the presence of no binaries in the bulge.

7. THE STELLAR *M/L* OF THE GALACTIC BULGE

The stellar M/L is an important parameter of a stellar population and depends on its IMF. We used the mass function derived in this work and the total luminosity of stars observed in the SWEEPS field to estimate the stellar M/L of the Galactic bulge in the $F814W$ and the $F606W$ filters. We obtain a total mass for bulge stars in the SWEEPS field included in the mass range adopted to estimate the IMF, $0.16 \leqslant M/M_{\odot} \leqslant 1.0$, of $137{,}527 \pm 23{,}400\ M_{\odot}$. By extrapolating the IMF with a power-law slope of $\alpha = -1.25$ down to the hydrogen burning limit, we get an extra mass of $14{,}310 \pm 2{,}400\ M_{\odot}$, for a total mass of $\approx 152{,}000 \pm 23{,}500\ M_{\odot}$ included in the $0.10 \leqslant M/M_{\odot} \leqslant 1.0$ mass range. Uncertainties take into account the error budget of the derived IMF. A constant mass of $1.0\ M_{\odot}$ is assumed for bulge sub- and red-giant stars and red clump stars, for a total mass of $4{,}116\ M_{\odot}$. We do not take into account the mass loss along the RGB, but since the total mass of the giants is already very small compared to the mass of the MS stars, this has no effect on the final derivation of the *M/L*.We then assume that the IMF of the Galactic bulge has a constant Salpeter power-law slope for masses larger than $1.0\ M_{\odot}$ and up to $120\ M_{\odot}$, and we integrate the IMF to obtain the number of stars that formed in this mass range. To estimate the mass currently in stellar remnants in the bulge we follow the prescriptions of Percival et al. (2009): stars with mass (i) $1 < M/M_{\odot} \leqslant 10$, the remnant is a white dwarf; (ii) $10 < M/M_{\odot} \leqslant 25$, the remnant is a neutron star, and (iii) $M > 25\ M_{\odot}$, the remnant is a black hole. In order to estimate the mass of white dwarf remnants, we used the initial-to-final mass relation by Salaris et al. (2009), $M_f = 0.084\ M_i + 0.466$ for initial masses less than $7\ M_{\odot}$ and a constant final mass of $1.3\ M_{\odot}$ for initial masses in the range $7 < M/M_{\odot} \leqslant 10$, obtaining a total mass in white dwarfs of $53{,}912 \pm 9{,}200\ M_{\odot}$. For neutron stars we assumed a constant mass of $1.4\ M_{\odot}$ and for black holes a mass equal to $1/3$ of the initial mass, obtaining total remnant masses of $3{,}905 \pm 600$ and $11{,}151 \pm 1{,}900\ M_{\odot}$ for neutron stars and black holes, respectively. By using the aforementioned values we found that the total stellar mass in the bulge SWEEPS field is $M = 228{,}814 \pm 25{,}300\ M_{\odot}$.

We estimated the flux emitted by bulge stars in the SWEEPS field by using the PM cleaned photometric catalog corrected for the total fraction of stars and for completeness. We thus obtained a total luminosity of $L_{F814W} \approx 104{,}000 \pm 2{,}000\ L_{\odot}$ and $L_{F606W} \approx 71{,}000 \pm 1{,}400\ L_{\odot}$. The stellar mass-to-light values based on our IMF and the photometric catalog for the SWEEPS field are then $M/L_{F814W} = 2.2 \pm 0.3$ and $M/L_{F606W} = 3.2 \pm 0.5$.

Table 3
Stellar Mass Estimates and Mass-to-light Values for the Galactic Bulge for Different Assumed IMF Slopes for $M > 1\ M_{\odot}$

α	Stellar Mass	M/L_{F814W}	M/L_{F606W}
Salpeter	$228{,}814 \pm 25{,}300$	2.2 ± 0.3	3.2 ± 0.5
-2.0	$254{,}505 \pm 28{,}100$	2.4 ± 0.4	3.6 ± 0.6
-2.7	$219{,}079 \pm 24{,}200$	2.1 ± 0.3	3.1 ± 0.5

We estimated the stellar mass included in our field by also using two other assumptions for the mass distribution at masses larger than $1\ M_{\odot}$: constant slopes of $\alpha = -2.0$ and of $\alpha = -2.7$. In the first case, we obtain a larger total stellar mass, $M = 254{,}505 \pm 28{,}100$, and larger mass-to-light values, $M/L_{F814W} = 2.4 \pm 0.4$ and $M/L_{F606W} = 3.6 \pm 0.6$, while in the second case we obtain smaller values, $M = 219{,}079 \pm 24{,}200$, $M/L_{F814W} = 2.1 \pm 0.3$ and $M/L_{F606W} = 3.1 \pm 0.5$. The total mass of the observed field and the stellar mass-to-light values estimated for the different cases are listed in Table 3.

Finally, we also explored a more theoretical route and we computed the average bulge luminosity in the SWEEPS field by using two different synthetic population codes by Cignoni et al. (2013) and BASTI. For both simulations we generated a fake stellar population with properties resembling those in the Galactic bulge: solar metallicity, constant star formation rate between 12 and 10 Gyr, our IMF, a binary fraction of 50%, distance modulus of 14.45 and reddening $E(B-V) = 0.5$.

In the first case we used the latest PARSEC stellar models (Bressan et al. 2012). Simulations were run until the number of stars in the magnitude range $20 \leqslant F606W \leqslant 22$ matched the observed number ($\sim$25,000 stars). This experiment was repeated 1,000 times. We found average values of $L_{F606W} \sim 58{,}900$ and $L_{F814W} \sim 92{,}800$. In order to evaluate the effect of metallicity dispersion we also tested different Z values, namely 0.008 and 0.03, corresponding to the metal-poor and metal-rich peaks of the metallicity distribution of the considered field. In these cases we found $L_{F606W} \sim 70{,}800$ and $L_{F814W} \sim 101{,}600$

for the former metallicity, and $L_{F606W}\sim$ 53,800 and $L_{F814W}\sim$ 87,500 for the latter. As expected, lowering the metallicity causes an increase in the luminosity of the system. Interestingly enough, luminosity values estimated for the lower metallicity, $Z = 0.008$, agree quite well with the observed values, while values for the higher metallicities are systematically lower than our flux estimates. A part of this discrepancy may be due to the possibility that a few very bright thin-disk stars are still contaminating our data, raising the inferred luminosities. In addition, the actual PARSEC models miss the asymptotic giant branch stellar phase, hence the predicted luminosities are likely to be underestimated.

We repeated the same experiment using the BASTI models for the three different metallicites, and obtained L_{F606W} and L_{F814W} values as ∼74,500 and ∼103,000 for Z = 0.008, ∼62,500, and ∼89,700 for Z = 0.02, and ∼57,200 and ∼86,200 for Z = 0.03. In this case the luminosity estimates for the lower metallicity are also in very good agreement with the observed values, while the luminosities obtained for the solar and higher metallicites are systematically lower. On the other hand, the luminosity estimates for the three metallicites based on the two different sets of models agree very well. Summarizing, we found a stellar *M/L* included in the range $2.1 < M/L_{F814W} < 2.4$ and $3.1 < M/L_{F606W} < 3.6$ according to different assumption on the slope of the IMF for masses larger than $1M_{\odot}$. These are likely to be slightly lower estimates of the real stellar mass-light budget of bulge since a few bright disk stars might still be contaminating our luminosity estimate. These values agree quite well, within the uncertainties, with the estimates provided by ZO00 in the Johnson *V* filter, $M/L_V \sim 3.4$, by using their IMF with a single slope of $\alpha = -1.33$ below 1 $M_{\odot}$, and by assuming a constant Salpeter IMF for stars more massive than 1 $M_{\odot}$.

8. MICROLENSING OPTICAL DEPTH

Several thousand microlensing events have been detected to date toward the Galactic bulge, mainly by the OGLE (Udalski et al. 2015) and MOA collaborations (Bond et al. 2001; Sako et al. 2008; Sumi et al. 2013). These microlensing events have been used by several investigators to derive the total mass budget as well as the mass function of the lenses.

Paczynski et al. (1994), based on a small number of microlensing events, noticed that the observed microlensing optical depth is in excess of the theoretical estimates, indicating a much higher efficiency for microlensing by either bulge or disk lenses. This issue has been further investigated in recent years by several groups (Sumi et al. 2013; Wyrzykowski et al. 2015). A helpful hint comes from the latest study by Wyrzykowski et al., which shows a dependence of the mean microlensing timescale on the Galactic latitude. This signals an increasing contribution from disk lenses closer to the plane relative to the height of the disk, which needs to be taken into account in the estimation of timescales and optical depths.

Since the timescale of the microlensing event is proportional to the square root of the mass of the lens, the timescales can be used for a statistical estimate of the mass function of the lenses. Zhao et al. (1995) and Han & Gould (1996) used this approach and reported a mass function with a slope of −2.0 and a cutoff at $\sim 0.1M_{\odot}$. Calchi Novati et al. (2008) also attempted to fit the observed timescales of the microlensing events with a power-law distribution of lens masses and obtained a slope of −1.7 for the distribution. As pointed out by ZO00, there may be an extra bias in the observed timescales due to blending in the ground-based observations, which causes the times scales to appear shorter than they actually are. This leads to an underestimation of the lens masses. Even so, the derived slope from microlensing observations is in between the two slopes of $\alpha = -2.41$ and −1.25 derived here, and thus seems consistent. It would be interesting to extend this microlensing analysis to the currently available list of all the observed microlensing events.

Finally, we note that the microlensing optical depth comes not only from the living MS stars, but also from the white dwarfs, neutron stars and black holes. The *M/L* derived in this paper should help in deriving a more correct estimate of the microlensing optical depth.

9. DISCUSSION AND CONCLUSIONS

We have derived the IMF of the pure bulge component down to 0.15 $M_{\odot}$. The Galactic bulge IMF can be fitted by two power laws, one with a steeper slope $\alpha = -2.41 \pm 0.50$ for $M \geqslant 0.56$ $M_{\odot}$, and another with a shallower slope $\alpha = -1.25 \pm 0.19$ for the lower masses. A log-normal function fits the IMF too, with a characteristic mass of $M_c = 0.25 \pm 0.07$ and $\sigma = 0.50 \pm 0.01$.

The slope of the IMF at high masses is mildly affected by the assumption on the fraction of unresolved binaries in the bulge or the distribution of their mass ratios. The high-mass slope ranges from $\alpha = -2.25 \pm 0.50$ for no binaries to $\alpha = -2.62 \pm 0.52$ for 100% of binaries in the bulge. On the other hand, the slope at lower masses changes significantly, ranging from $\alpha = -0.89 \pm 0.20$ for no binaries to $\alpha = -1.55 \pm 0.20$ for 100% of binaries.

As we noted earlier, the slope of the IMF at the very low-mass range is crucial in estimating the mass budget of the Galactic bulge which contains ≈20% of the mass of the Galaxy. Our deep *HST* observations obtained over a timescale of ∼9 years allowed us to derive the mass function of the pure bulge component even in this low-mass range, which was previously not possible.

The shape of the Galactic bulge IMF we derived in this work is in good agreement, within the uncertainties, with the IMFs derived previously by HO98 for the Baade's window, but our mass function extends to lower masses and it is purely based on bulge members with negligible contamination from disk stars. On the other hand, our IMF not corrected for the presence of unresolved binaries shows a slightly shallower slope compared to ZO00 IMF (−1.14 versus −1.33). This difference could be due to a small residual contamination by disk stars of the ZO00 sample, or to some intrinsic differences in the stars in the field observed by ZO00 and stars in the SWEEPS field.

Our bulge IMF is in very good agreement with the mass function derived for the Galactic disk by Kroupa (2001) and Chabrier (2003) in the entire mass range, while it is steeper in the VLM regime compared to the mass functions derived for the disk by Gould et al. (1997) and Reid et al. (2002). The PDMFs derived in the more recent studies of Covey et al. (2008) and Bochanski et al. (2010) agree quite well with our IMF for the Galactic bulge in the high-mass range, but they still show a shallower slope in the low mass range.

The characterization of the IMF in different stellar environments is fundamental for investigating if the IMF has a dependence on the stellar metallicity and/or age. The recent work of Kalirai et al. (2013) showed that the IMF of the Small

Magellanic Cloud (SMC, $-1.5 \lesssim$ [Fe/H] $\gtrsim -1.0$) is shallower than the Salpeter mass function, $\alpha = -1.9$, down to $\approx 0.4 M_{\odot}$, and does not show evidence for a turn-over in the VLM regime. Furthermore, Geha et al. (2013) showed that the IMF of two metal-poor ([Fe/H] < -2.0) ultra faint galaxies, Hercules and Leo IV, are even shallower, having a slope in the range $\alpha = -1.2$–1.3 for masses larger than $\approx 0.5 M_{\odot}$. In the higher-mass range ($M > 0.5 M_{\odot}$) where the mass function of these galaxies is well measured, our bulge IMF is steeper than both the IMFs of the intermediate-metallicity environment of the SMC (-2.41 versus -1.9) and the metal-poor environment of the ultra-faint galaxies (-2.41 versus -1.3 to -1.2), pointing toward a variation of the IMF with the global average metallicity of the stellar population. However, more data are needed to sample the IMF down to lower masses, i.e., 0.1 $M_{\odot}$, in the different environments, to confirm this preliminary result.

We then used the derived IMF to estimate the stellar *M/L* of the Galactic bulge. We obtained for the two filters, values included in the range $2.1 < M/L_{F814W} < 2.4$ and $3.1 < M/L_{F606W} < 3.6$ according to different assumption on the slope of the IMF for masses larger than $1 M_{\odot}$.

The shape of the mass function derived from microlensing observations has large uncertainties but is in consistent with the observed bulge IMF presented here.

This study was supported by NASA through grants GO-9750 and GO-12586 from the Space Telescope Science Institute, which is operated by AURA, Inc., under NASA contract NAS 5-26555. SC and RB thank financial support from PRIN-INAF2014 (PI: S. Cassisi). We thank the anonymous referee for helpful suggestions which led to an improved version of the paper.

REFERENCES

Bedin, L. R., Cassisi, S., Castelli, F., et al. 2005, MNRAS, 357, 1038
Bedin, L. R., Salaris, M., Piotto, G., et al. 2009, ApJ, 697, 965
Bensby, T., Yee, J. C., Feltzing, S., et al. 2013, A&A, 549, A147
Bochanski, J. J., Hawley, S. L., Covey, K. R., et al. 2010, AJ, 139, 2679
Bond, I. A., Abe, F., Dodd, R. J., et al. 2001, MNRAS, 327, 868
Bressan, A., Marigo, P., Girardi, L., et al. 2012, MNRAS, 427, 127
Calamida, A., Sahu, K. C., Anderson, J., et al. 2014, ApJ, 790, 164
Calchi Novati, S., de Luca, F., Jetzer, P., Mancini, L., & Scarpetta, G. 2008, A&A, 480, 723
Cardelli, J. A., Clayton, G. C., & Mathis, J. S. 1989, ApJ, 345, 245
Cassisi, S., Castellani, V., Ciarcelluti, P., Piotto, G., & Zoccali, M. 2000, MNRAS, 315, 679
Cassisi, S., & Salaris, M. 2011, ApJL, 728, L43
Cassisi, S., Salaris, M., Anderson, J., et al. 2009, ApJ, 702, 1530
Cassisi, S., Salaris, M., Pietrinferni, A., Vink, J. S., & Monelli, M. 2014, A&A, 571, A81
Chabrier, G. 2003, PASP, 115, 763
Chabrier, G. 2005, in The Initial Mass Function 50 Years Later, Vol. 327, ed. E. Corbelli, F. Palla & H. Zinnecker, 41
Cignoni, M., Cole, A. A., Tosi, M., et al. 2013, ApJ, 775, 83
Clarkson, W., Sahu, K., Anderson, J., et al. 2008, ApJ, 684, 1110
Covey, K. R., Hawley, S. L., Bochanski, J. J., et al. 2008, AJ, 136, 1778
Duquennoy, A., & Mayor, M. 1991, A&A, 248, 485
Dutton, A. A., Treu, T., Brewer, B. J., et al. 2013, MNRAS, 428, 3183
Fukugita, M., Hogan, C. J., & Peebles, P. J. E. 1998, ApJ, 503, 518
Geha, M., Brown, T. M., Tumlinson, J., et al. 2013, ApJ, 771, 29
Gonzalez, O. A., Rejkuba, M., Zoccali, M., et al. 2011, A&A, 530, A54
Gould, A., Bahcall, J. N., & Flynn, C. 1997, ApJ, 482, 913
Han, C., & Gould, A. 1996, ApJ, 467, 540
Hauschildt, P. H., Allard, F., Ferguson, J., Baron, E., & Alexander, D. R. 1999, ApJ, 525, 871
Hill, V., Lecureur, A., Gómez, A., et al. 2011, A&A, 534, A80
Holtzman, J. A., Watson, A. M., Baum, W. A., et al. 1998, AJ, 115, 1946
Johnson, C. I., Rich, R. M., Fulbright, J. P., Valenti, E., & McWilliam, A. 2011, ApJ, 732, 108
Johnson, C. I., Rich, R. M., Kobayashi, C., et al. 2013, ApJ, 765, 157
Kalirai, J. S., Anderson, J., Dotter, A., et al. 2013, ApJ, 763, 110
Kroupa, P. 2001, MNRAS, 322, 231
Kroupa, P., Gilmore, G., & Tout, C. A. 1991, MNRAS, 251, 293
Kroupa, P., & Tout, C. A. 1997, MNRAS, 287, 402
Kroupa, P., Tout, C. A., & Gilmore, G. 1993, MNRAS, 262, 545
McKee, C. F., & Ostriker, E. C. 2007, ARA&A, 45, 565
Nataf, D. M., Gould, A., Fouqué, P., et al. 2013, ApJ, 769, 88
Ness, M., Freeman, K., Athanassoula, E., et al. 2013, MNRAS, 430, 836
Oosterhoff, P. T., & Ponsen, J. 1968, BANS, 3, 79
Paczynski, B., Stanek, K. Z., Udalski, A., et al. 1994, ApJL, 435, L113
Percival, S. M., Salaris, M., Cassisi, S., & Pietrinferni, A. 2009, ApJ, 690, 427
Pietrinferni, A., Cassisi, S., Salaris, M., & Castelli, F. 2004, ApJ, 612, 168
Pietrinferni, A., Cassisi, S., Salaris, M., & Castelli, F. 2006, ApJ, 642, 797
Portail, M., Wegg, C., Gerhard, O., & Martinez-Valpuesta, I. 2015, MNRAS, 448, 713
Raghavan, D., McAlister, H. A., Henry, T. J., et al. 2010, ApJS, 190, 1
Reid, I. N., & Gizis, J. E. 1997, AJ, 113, 2246
Reid, I. N., Gizis, J. E., & Hawley, S. L. 2002, AJ, 124, 2721
Sahu, K. C., Casertano, S., Bond, H. E., et al. 2006, Natur, 443, 534
Sako, T., Sekiguchi, T., Sasaki, M., et al. 2008, ExA, 22, 51
Salaris, M., Serenelli, A., Weiss, A., & Miller Bertolami, M. 2009, ApJ, 692, 1013
Salpeter, E. E. 1955, ApJ, 121, 161
Sirianni, M., Jee, M. J., Benítez, N., et al. 2005, PASP, 117, 1049
Sofue, Y., Honma, M., & Omodaka, T. 2009, PASJ, 61, 227
Sumi, T., Bennett, D. P., Bond, I. A., et al. 2013, ApJ, 778, 150
Treu, T., Dutton, A. A., Auger, M. W., et al. 2011, MNRAS, 417, 1601
Udalski, A., Szymański, M. K., & Szymański, G. 2015, AcA, 65, 1
Vazdekis, A., Coelho, P., Cassisi, S., et al. 2015, MNRAS, 449, 1177
Wyrzykowski, Ł., Rynkiewicz, A. E., Skowron, J., et al. 2015, ApJS, 216, 12
Zhao, H., Spergel, D. N., Rich, R. M., et al. 1995, ApJL, 440, L13
Zoccali, M., Cassisi, S., Frogel, J. A., et al. 2000, ApJ, 530, 418
Zoccali, M., Hill, V., Lecureur, A., et al. 2008, A&A, 486, 177
Zoccali, M., Renzini, A., Ortolani, S., et al. 2003, A&A, 399, 931